

Supporting Information:

Gas phase composition and secondary organic aerosol formation from gasoline direct injection vehicles investigated in batch and flow reactors: effects of prototype gasoline particle filters.

5 Simone M. Pieber¹, Nivedita K. Kumar¹, Felix Klein¹, Pierre Comte², Deepika Bhattu¹, Josef Dommen¹,
Emily A. Bruns¹, Dogushan Kilic¹, Imad El Haddad¹, Alejandro Keller³, Jan Czerwinski², Norbert
Heeb⁴, Urs Baltensperger¹, Jay G. Slowik¹ and André S. H. Prévôt¹

¹Paul Scherrer Institute, Laboratory of Atmospheric Chemistry, CH-5232 Villigen, Switzerland

²Bern University of Applied Sciences, CH-2560 Nidau, Switzerland

10 ³Empa Material Science and Technology; CH-8600 Dübendorf, Switzerland

⁴University of Applied Sciences Northwestern Switzerland; CH-5210 Windisch, Switzerland

Correspondence to: andre.prevot@psi.ch

1 Emission Factors (EFs)

Emission factors from batch experiments are calculated based on a carbon mass balance as described in (Platt et al., 2013);

15 (Platt et al., 2017) (Eq. (S1)), where P is the species of interest, w_c the carbon fraction (0.85) of the fuel and CO_2 and CO , NMOC and eBC are in units of carbon mass.

$$\text{EF} = \frac{\Delta P}{\Delta \text{CO}_2 + \Delta \text{CO} + \Delta \text{NMOC} + \Delta \text{eBC}} * w_c \quad (\text{S1})$$

20 Regulatory emission factors from the test bench were provided in accordance with the ECE Regulation No. 83, the fuel consumption of the vehicle in accordance with the ECE Regulation No. 101 and the effective fuel density (0.75 kg L^{-1}).

2 OFR data quality (OH exposure, non-OH losses and NO_x influence)

Several recent studies ((Li et al., 2015);(Peng et al., 2016;Peng et al., 2015)) have estimated the contribution of reaction processes in the OFR other than OH radicals across a range of operating conditions (residence time, water vapor availability, 25 and external OH reactivity (OHR_{ext}), which is the available OH-reactive material). These non-OH processes include reaction with photons (185 nm, 254 nm), and reactions with oxygen allotropes (excited oxygen atoms ($\text{O}({}^1\text{D})$)), ground state oxygen atoms ($\text{O}({}^3\text{P})$), ozone (O_3)) were identified as relevant loss processes to precursor molecules. Under certain operating conditions, also suppression of OH formation is critical. We applied a previously published model ((Peng et al., 2016;Peng et

al., 2015)) to estimate competing reaction with OH and loss of precursor molecules by non-OH sources, and estimated the influence of NOx based on (Peng and Jimenez, 2017)). Details on model input parameters are presented in the following:

(a) **OFR-from-SC** (see results in Figure S11). As input to the model we used $OHR_{ext}=100 \text{ s}^{-1}$, $[O_3]=1.97 \times 10^{14} \text{ molec cm}^{-3}$ (corresponding to 8 ppm at 100% UV intensity) a water mixing ratio=0.01 (1% absolute humidity, corresponding to 50% RH at 25°C) and a residence time=100 sec. O_3 measured at our reactor output for 70% UV intensity was $0.74 \times 10^{14} \text{ molec cm}^{-3}$ (3 ppm), and at 50% UV intensity $0.17 \times 10^{14} \text{ molec cm}^{-3}$ (0.7 ppm). OHR_{ext} was calculated following Eq. (S2).

$$OHR_{ext} = \sum_i (c_{NMOC,i} * k_{OH,NMOC,i}); \quad i=\text{BENZ, TOL, XYL/EBENZ, C3-BENZ, CO, BuOH-D9} \quad (S2)$$

where k_{OH} of benzene (BENZ), toluene (TOL), xylene/ethylbenzene (XYL/EBENZ), C3-benzene (C3-BENZ) are given in Table 2 (main text); here we applied $k_{OH,BENZ}=1.22 \times 10^{-12}$, $k_{OH,TOL}=5.63 \times 10^{-12}$, $k_{OH,XYL/EBENZ}=(7-23) \times 10^{-12}$, $k_{OH,C3-BENZ}=(6-57) \times 10^{-12}$, $k_{OH,CO}=1.5 \times 10^{-13}$ (IUPAC)), $k_{OH,BuOH-D9}=3.4 \times 10^{-12}$ (Barmet et al., 2012); all in $\text{cm}^3 \text{ molec s}^{-1} \text{ s}^{-1}$ and used a concentration average of expt A1 of $c_{BENZ}=4 \times 10^{11}$, $c_{TOL}=1 \times 10^{12}$, $c_{XYL/EBENZ}=8 \times 10^{11}$, $c_{C3-BENZ}=2 \times 10^{11}$, $c_{CO}=(3-7) \times 10^{14}$, $c_{BuOH-D9}=(3.7-7.4) \times 10^{11}$; all in molec cm^{-3} as input. This results in an OHR_{ext} of $70-100 \text{ s}^{-1}$. Based on these input parameters, the model (Peng et al., 2016) predicted an $[\text{OH}]_{\text{exposure}}$ (OH concentration integrated over time, see discussion in main text “OH exposure estimation”, in $\text{molec cm}^{-3} \text{ s}$) in the OFR of

$$\begin{aligned} \text{UV100\%:} \quad & [\text{OH}]_{\text{exposure}} = (10-13) \times 10^{11} \\ \text{UV70\%:} \quad & [\text{OH}]_{\text{exposure}} = (2.4-3.1) \times 10^{11} \\ \text{UV50\%:} \quad & [\text{OH}]_{\text{exposure}} = (0.35-0.48) \times 10^{11}. \end{aligned}$$

The estimated $[\text{OH}]_{\text{exposure}}$ (in $\text{molec cm}^{-3} \text{ s}$) and OH concentration (in molec cm^{-3}), $[\text{OH}]$, based on the experimental measurements of the decay of BuOH-D9 correspond instead to

$$\begin{aligned} \text{UV100\%:} \quad & [\text{OH}]_{\text{exposure}} = (3.0-5.8) \times 10^{11}, \text{ i.e. } [\text{OH}] = (2.7-5.2) \times 10^9 \\ \text{UV70\%:} \quad & [\text{OH}]_{\text{exposure}} = (1.6-2.5) \times 10^{11}, \text{ i.e. } [\text{OH}] = (1.4-2.2) \times 10^9 \\ \text{UV50\%:} \quad & [\text{OH}]_{\text{exposure}} = (0.31-0.49) \times 10^{11}, \text{ i.e. } [\text{OH}] = (0.28-0.44) \times 10^9, \end{aligned}$$

The ratio of OH (measured) to O_3 (measured) remained relatively constant at our test points (OH/O_3 at 100\%: $(1.4-2.6) \times 10^{-5}$, $(1.9-3.0) \times 10^{-5}$ at 70\%, $(1.7-2.6) \times 10^{-5}$ at 50\%). The corresponding OH information derived from measurements in the SC is an $[\text{OH}]_{\text{exposure}}$ of $1.4 \times 10^{11} \text{ molec cm}^{-3} \text{ s}$ at the maximum aging time (after around 2 hours), at a constant $[\text{OH}] = 2 \times 10^7 \text{ molec cm}^{-3} \text{ s}$.

Non-OH loss analysis (Figure S11) predicts losses of aromatic hydrocarbons as SOA precursors to up to 10-15% by UV185 nm and UV254 nm, but no impact of O_3 , (neither $O(^1D)$ or $O(^3P)$) for the OFR-from-SC conditions. This only refers to the reactive interaction of OH vs. the excitation by UV, and does not allow conclusions on the formation of SOA. Also 5 chemistry initiated by UV185 or UV254 may lead to the formation of SOA. Additionally, it does not suggest any conclusions about the interaction of O_3 with double bonds made available by first ring-opening reactions. However, as our results suggest that yields and O:C ratios between OFR and SC compare well, we believe that the additional impact of photolysis and O_3 on the initial SOA precursors in the OFR is negligible in our OFR-from-SC experiments. Potential effects 10 of O_3 on first generation products are not taken into account. Under those diluted conditions (initial NO < 100 ppb), we regard the experiments in OFR as low NO conditions (Peng and Jimenez, 2017). The dominant SOA precursors found in the 15 exhaust are not reactive towards NO_3 radicals that can be formed in the OFR; potential effects on first generation products are not taken into account. A full discussion of this issue is presented in (Peng and Jimenez, 2017), who state that under conditions with several hundreds of ppb of NO, an NO_3 exposure-to- OH exposure of 0.1-1 may be reached, with potential impacts on first generation oxidation products (such as phenolic compounds).

15

(b) Time-Resolved OFR (see results in Figure S12). As input to the model we used $OHR_{ext}=1000\text{ s}^{-1}$ (for experiments conducted with 1 dilution step, 2014) and $OHR_{ext}=100\text{ s}^{-1}$ for experiments with 2 dilution steps (2015), $[O_3]=1.97\times 10^{14}\text{ molec cm}^{-3}$, a water mixing ratio=0.005 (0.5% absolute humidity, corresponding to ~20% RH at 25°C) and a residence time=100 s. Based on these parameters, the model (Peng et al., 2016) predicts $[OH]_{exposure}=(5.9)\times 10^{10}\text{ molec cm}^{-3}\text{ s}$. For the 20 2015 experiments ($OHR_{ext}=100\text{ s}^{-1}$), results from (a) apply (Figure S11). Due to the lower dilution ratio in the time-resolved OFR experiments in 2014, however, a significant fraction of the emissions (up to 50-60% of the ArHC) are lost with UV185 and UV254 nm radicals instead of OH, as a high OHR_{ext} leads to OH suppression in the reactor, making non-OH processes 25 relatively more important. Also $O(^1D)$ and $O(^3P)$ reduce ArHC by ca 10-20% under these conditions (Figure S12). Potential effects of O_3 on first generation products are not taken into account. As detailed in (Peng and Jimenez, 2017), the NO_x/VOC ratio is a function of the driving cycle. Under conditions with insufficient dilution during time-resolved measurements 30 conducted in 2014, we additionally cannot exclude the influence of NO and NO_3 during simulated photochemical aging as NO levels reached “a few ppm levels” during the initial phases of the test cycles. During time-resolved measurements conducted in 2015 (double dilution), NO levels were on the order of a few hundreds of ppb and based on this we estimate no significant impact on our time-resolved SOA profiles, as well as the integrated SOA mass on first generation products. Again, for a full discussion of this issue please refer to (Peng and Jimenez, 2017), who state that under conditions with 35 several hundreds of ppb of NO, an NO_3 exposure-to- OH exposure of 0.1-1 may be reached, with potential impacts on first generation oxidation products (such as phenolic compounds).

Quantitative use of OFR data (OFR-from-SC and time-resolved OFR). SOA yields analysis in the main text is based on SC and OFR-from-SC experiments only. SOA emission factors (EF) are calculated based on SC and OFR-from-SC experiments. Additionally, time-resolved data from 2015 collected with GDI4 were integrated to derived EFs labelled “Online, OFR100%” in the main text (Sections 3.1, 3.2 and 3.4, and main text Figures 2b, Figure 4) and are comparable to 5 data derived from GDI4 SC experiments. Time-resolved SOA data from 2014 are not used quantitatively herein, due to instabilities with the OH exposure throughout the driving cycle (lower OH exposure during high emissions period as well as impact by photolysis and competing non-OH processes (i.e. high external OH reactivity (OHR_{ext} , see Figure S12, as well as ((Peng et al., 2015);(Peng et al., 2016); (Li et al., 2015)) and changing NO_x levels in the emissions as a function of driving 10 cycle with potential impact on the oxidation regime (high vs. low NO levels, see (Peng and Jimenez, 2017)). While these processes limit the use of time-resolved data collected in 2014 due to the low dilution ratio that was applied (only one-fold 15 dilution, i.e. 1 ejector dilutor, 1:8, and additional 1:2 at OFR entrance) and the resulting high OHR_{ext} ($>1000\text{ s}^{-1}$, see Eq. S2, and NO_x levels), data from 2015 are not significantly impacted. For data from 2015 (an example is given in Figure S14 for GDI4 in standard configuration and w/catGPF), such experimental artefacts were reduced by use of a higher dilution ratio (2 ejector dilutors in series, 2x 1:8 and additional 1:2 at OFR entrance, OHR_{ext} on the order of 100 s^{-1}). While we don’t rely on an absolute quantitative use of our time-resolved data from 2014, the relative profile (dominated by cold start) holds true regardless of these effects and is also confirmed in the 2015 data set (Figure S14) showing the same trends (largest SOA formation observed at cold engine start).

Figures (Supporting Information)

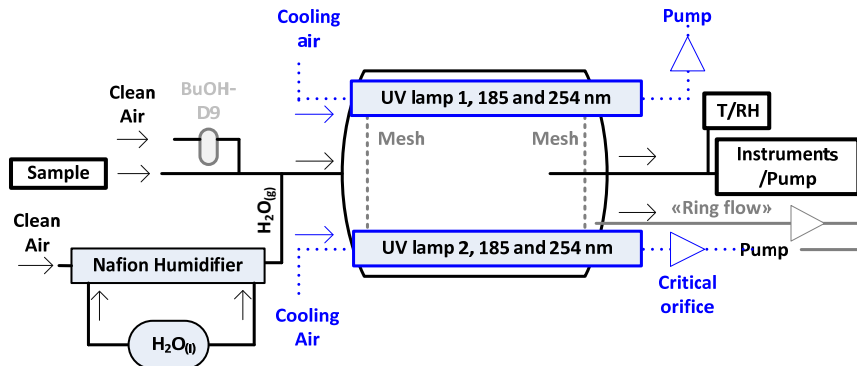


Figure S1. OFR schematic (not to scale). The OFR version deployed here was previously described in (Bruns et al., 2015). The reactor is a 0.015 m^3 , cylindrical glass chamber (0.46 m L, 0.22 m diameter) flanked by two UV lamps on the upper part of the reactor, each with discrete emission lines at 185 and 254 nm (BHK Inc.). The lamps are cooled by a constant flow of air, or N_2 . The incoming reactant flow is radially dispersed in the OFR by passing through a perforated mesh screen at the inlet flange. The flow through the OFR is determined by the flow pulled by instruments and pumps behind the reactor. The reactor is equipped with an injection system for water vapor (H_2O) and NMOCs (notably BuOH-D9, and selected precursor for single molecule testing). Water vapor is provided via a Nafion humidifier. Air is passing on one side of the Nafion membrane, collecting water vapor from the liquid on the other side of the membrane. In addition, other chemicals, such as BuOH-D9 (used as an OH tracer) can be injected by passing a small stream of clean air through a vial containing the liquid NMOC.

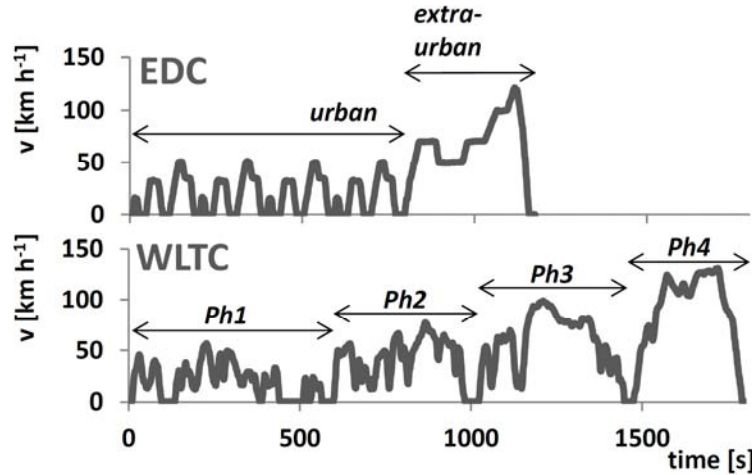


Figure S2. Speed profile of regulatory driving tests. Speed profile (v , in km h^{-1}) versus test time (in seconds) of EDC (new European driving cycle, top) and WLTC (world-wide light duty test cycle, class-3, bottom). While the EDC is characterized by two phase (an urban, and an extra-urban phase of highly repetitive characteristics) and lasts 20 min, the WLTC (class-3) is characterized by four phases at different speed levels (referred to as Phase (Ph) 1-4, or low, medium, high, and extra-high speed, respectively); it contains patterns of disruptive acceleration and deceleration, and lasts 30 min. The WLTC is believed to represent typical driving conditions around the world and was developed based on combination of collected in-use data and suitable weighting factors by an expert group from China, EU, India, Japan, South Korea, Switzerland and the USA.

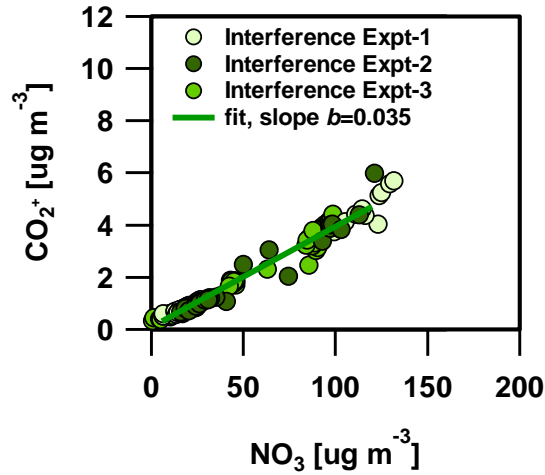


Figure S3. Ammonium nitrate (NH_4NO_3) interference on CO_2^+ (Pieber et al., 2016). The CO_2^+ signal (RIE=1) vs the NO_3 signal (RIE=1) from pure ammonium nitrate (NH_4NO_3) aerosol with $d_m=400$ nm from 3 calibration experiments. An orthogonal distance least squares fit yields a slope of $b=0.035$. Corrections were applied via the fragmentation table as noted in the main text.

10

15

20

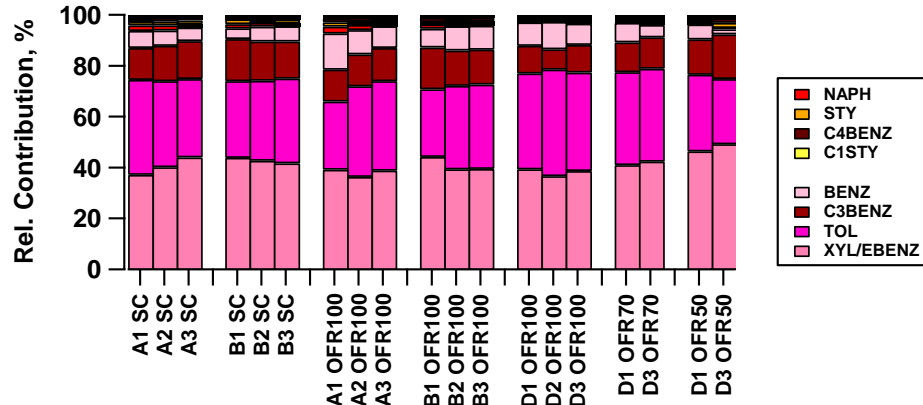


Figure S4. Reacted NMOC fraction in the SC (at t=2h after UV on), and the OFR at 100, 70 and 50% UV intensity (8 dominant ArHC). A-D identifiers refer to individual experiments (GDI 1 only). The max. OH exposure in the SC compares to an OH exposure of the OFR at 50-70% UV setting.

5

10

15

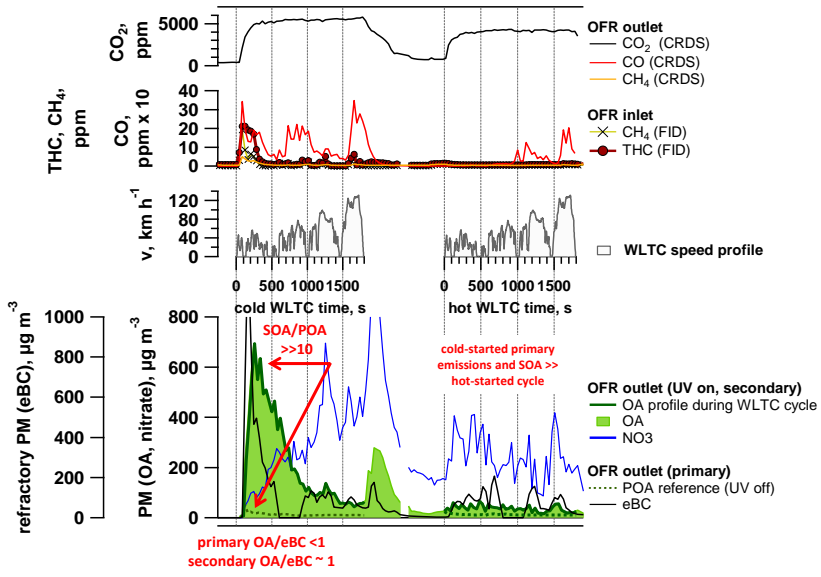


Figure S5. Time-resolved aging of emissions (WLTC) (GDI1, standard configuration, Expt A1). Cold and hot started WLTC of vehicle GDI1 (standard configuration). CO₂, CO, CH₄ (as measured by CRDS), THC and CH₄ (as measured by FID, note that the THC signal reaches its range limit at 20 ppm) are presented, together with organic aerosol (primary (denoted POA) and total (POA+SOA), denoted as OA). “OA profile during WLTC” highlights the measurement during the driving cycle, whereas OA shows the extended signal taking into account a delay due to the OFR residence time. Secondary nitrate aerosol (inorganic, ammonium nitrate, displayed is only NO₃), and primary equivalent black carbon (eBC). Note: data in these graphs are not normalized to CO₂, and have slightly different dilution ratios between cold- and hot-started cycle, as indicated by the CO₂ time-trace. Data reflect measured concentrations; no dilution corrections are applied. CRDS was diluted by a factor of 10 compared to FID and particle phase measurements.

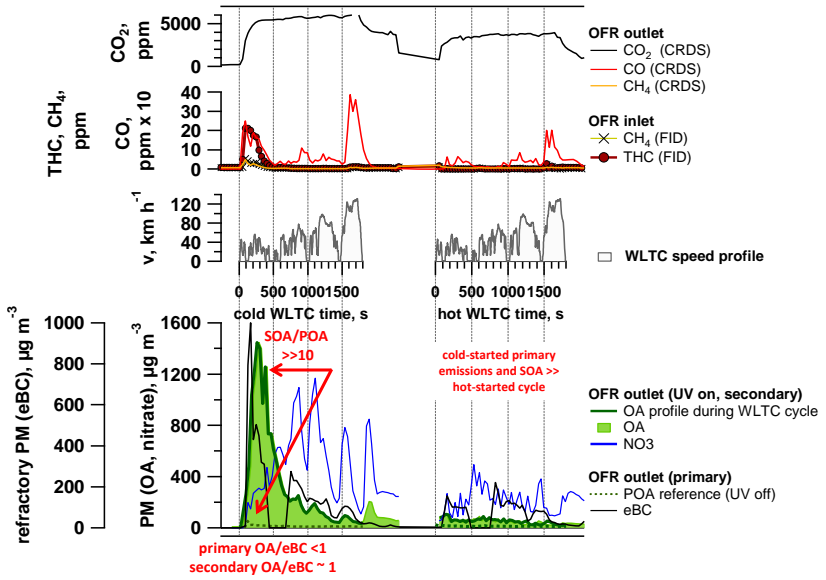


Figure S6. Time-resolved aging of emissions (WLTC) (GDI1, standard configuration, Expt A2, extended version of main text Figure 3). Cold and hot started WLTC of vehicle GDI1 (standard configuration). CO₂, CO, CH₄ (as measured by CRDS), THC and CH₄ (as measured by FID, note that the THC signal reaches its range limit at 20 ppm) are presented, together with organic aerosol (primary

5 (denoted POA) and total (POA+SOA), denoted as OA. “OA profile during WLTC cycle” highlights the measurement during the driving cycle, whereas OA shows the extended signal taking into account a delay due to the OFR residence time. Secondary nitrate aerosol (inorganic, ammonium nitrate, displayed is only NO₃), and primary equivalent black carbon (eBC). Note: data in these graphs are not normalized to CO₂, and have slightly different dilution ratios between cold- and hot-started cycle, as indicated by the CO₂ time-trace. Data reflect measured concentrations; no dilution corrections are applied. CRDS was diluted by a factor of 10 compared to FID and particle

10

15

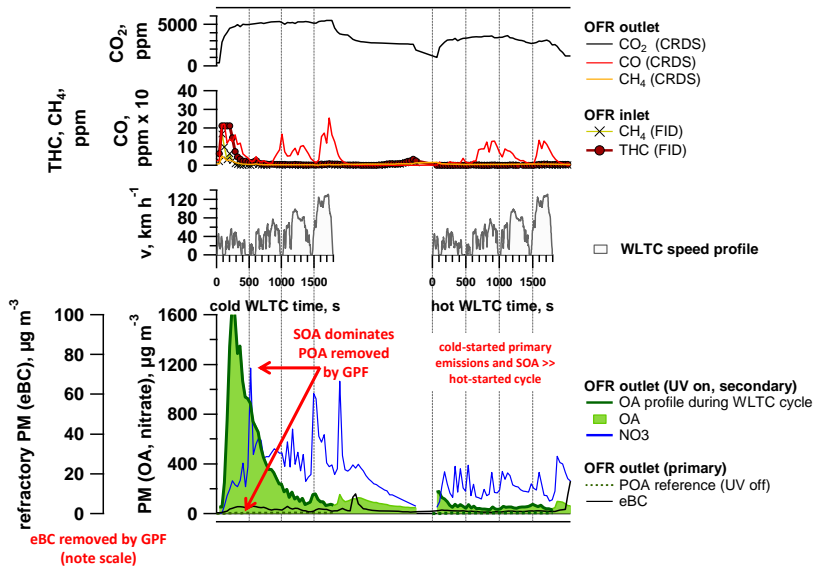


Figure S7. Time-resolved aging of emissions (WLTC) (GDI1 w/ GPF, Expt B1). Cold and hot started WLTC of vehicle GDI1 (w/GPF). CO₂, CO, CH₄ (as measured by CRDS), THC and CH₄ (as measured by FID, note that the THC signal reaches its range limit at 20 ppm) are presented, together with organic aerosol (primary (denoted POA) and total (POA+SOA), denoted as OA. “OA profile during

5 WLTC cycle” highlights the measurement during the driving cycle, whereas OA shows the extended signal taking into account a delay due to the OFR residence time. Secondary nitrate aerosol (inorganic, ammonium nitrate, displayed is only NO₃), and primary equivalent black carbon (eBC). Note: data in these graphs are not normalized to CO₂, and have slightly different dilution ratios between cold- and hot-started cycle, as indicated by the CO₂ time-trace. Data reflect measured concentrations; no dilution corrections are applied. CRDS was diluted by a factor of 10 compared to FID and particle phase measurements.

10

15

11

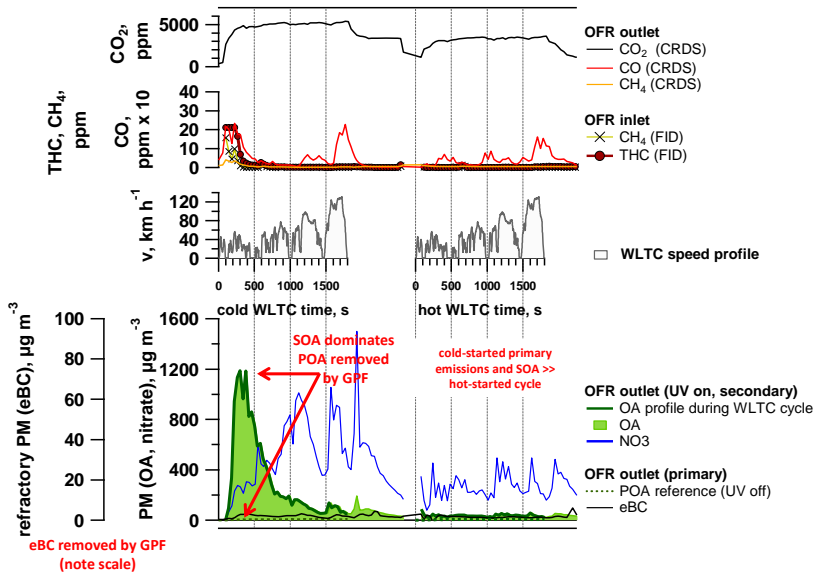


Figure S8. Time-resolved aging of emissions (WLTC) (GDI1 w/ GPF, Expt B2). Cold and hot started WLTC of vehicle GDI1 (w/GPF). CO₂, CO, CH₄ (as measured by CRDS), THC and CH₄ (as measured by FID, note that the THC signal reaches its range limit at 20 ppm) are presented, together with organic aerosol (primary (denoted POA) and total (POA+SOA), denoted as OA. “OA profile during WLTC cycle” highlights the measurement during the driving cycle, whereas OA shows the extended signal taking into account a delay due to the OFR residence time. Secondary nitrate aerosol (inorganic, ammonium nitrate, displayed is only NO₃), and primary equivalent black carbon (eBC). Note: data in these graphs are not normalized to CO₂, and have slightly different dilution ratios between cold- and hot-started cycle, as indicated by the CO₂ time-trace. Data reflect measured concentrations; no dilution corrections are applied. CRDS was diluted by a factor of 10 compared to FID and particle phase measurements.

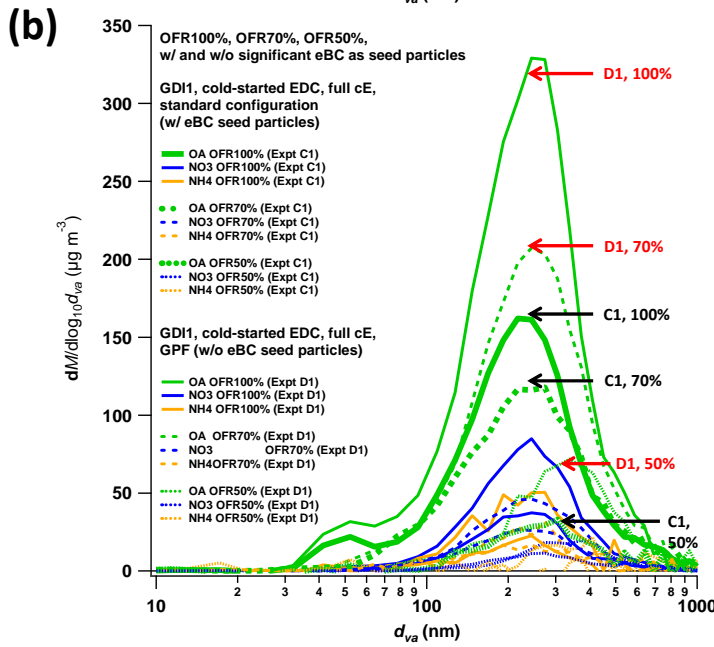
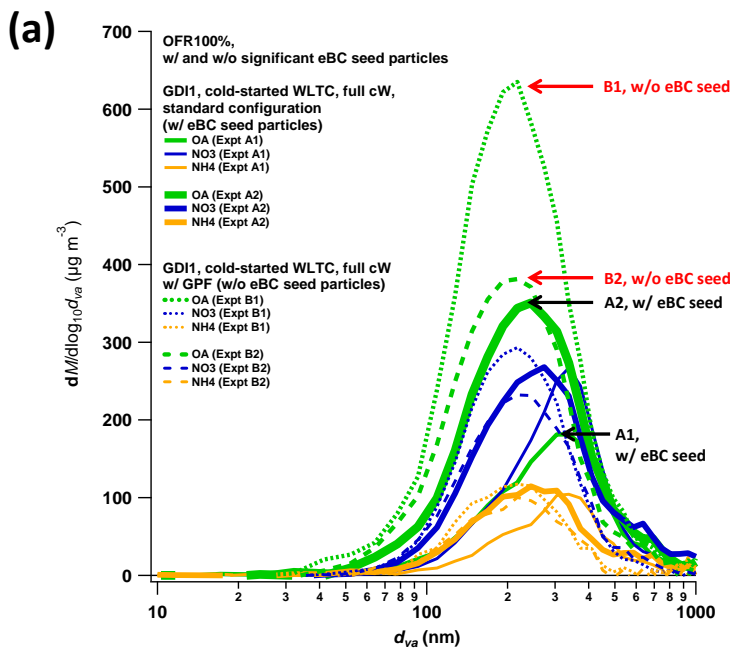


Figure S9. Particle size distributions for experiments from (a) WLTC and (b) EDC, measured behind the OFR-from-SC. All expts are OFR-from-SC tests leading to typically $200 \mu\text{g m}^{-3}$ ($\sim 100\text{--}500 \mu\text{g m}^{-3}$) SOA formed at 100%, down to $\sim 50 \mu\text{g m}^{-3}$ for 50% UV conditions. Expt A-D are identifiers for experiments referring to Table S4.

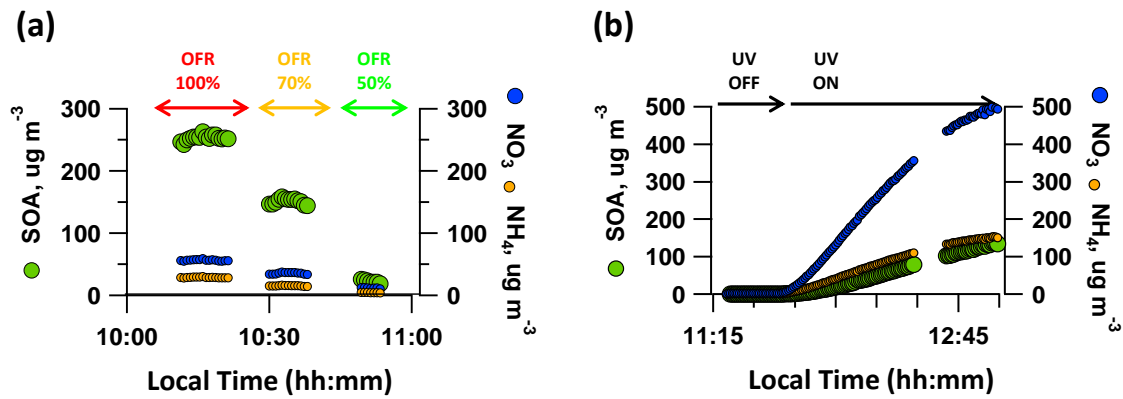


Figure S10. Bulk aerosol composition: OA, nitrate (denoted NO_3) and ammonium (denoted NH_4). Example of experiments in (a) 5 OFR-from-SC at varied UV intensities (Expt A1), local time in 30 min intervals, (b) SC (Expt B1), local time in 15 min intervals.

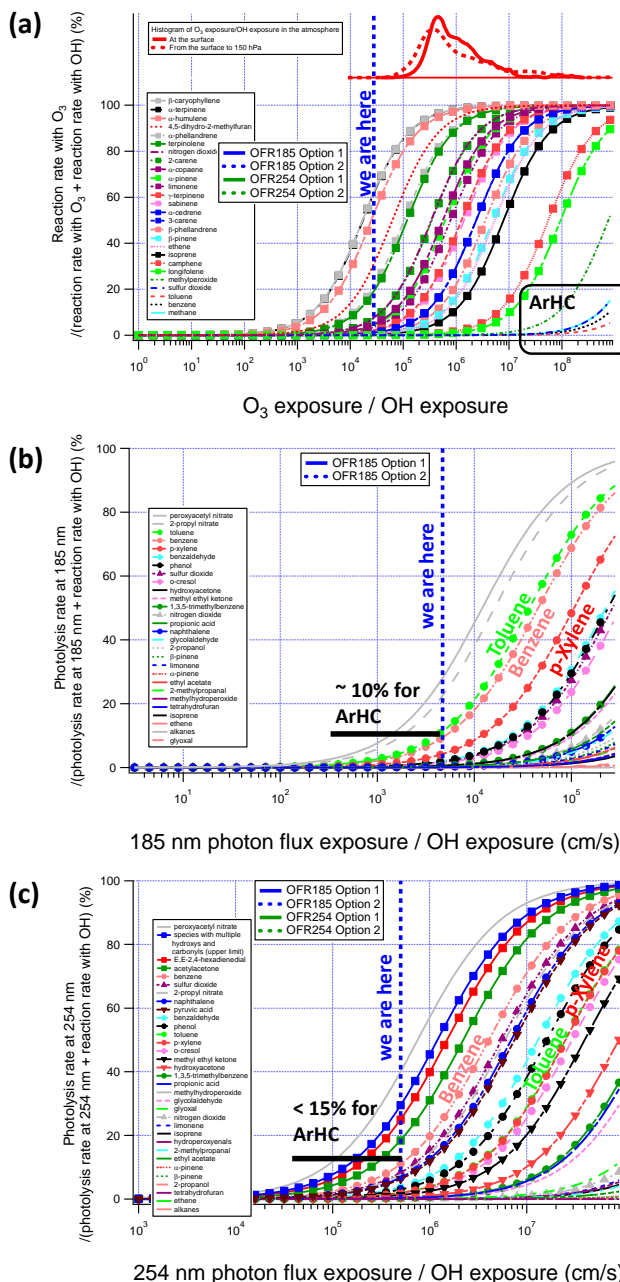


Figure S11. OFR-from-SC: non-OH loss estimation (Peng et al. OFR model (Peng et al., 2016)). Results are presented for OFR-from-SC Expts at 100% UV intensity, i.e. $[\text{OH}] = 2.7\text{--}5.2 \times 10^9 \text{ molec cm}^{-3}$. (a) O_3 , (b) 185 nm, (c) 254 nm; please refer to Peng et al. for the legend.(Peng et al., 2016). Input parameters to “2016-10-12_OFR_Exposures_Estimator_v2.3”: $\text{OHR}_{\text{ext}} = 100 \text{ s}^{-1}$, $[\text{O}_3] = 1.97 \times 10^{14} \text{ molec cm}^{-3}$, water mixing ratio = 0.01 (1% absolute humidity), residence time=100 sec

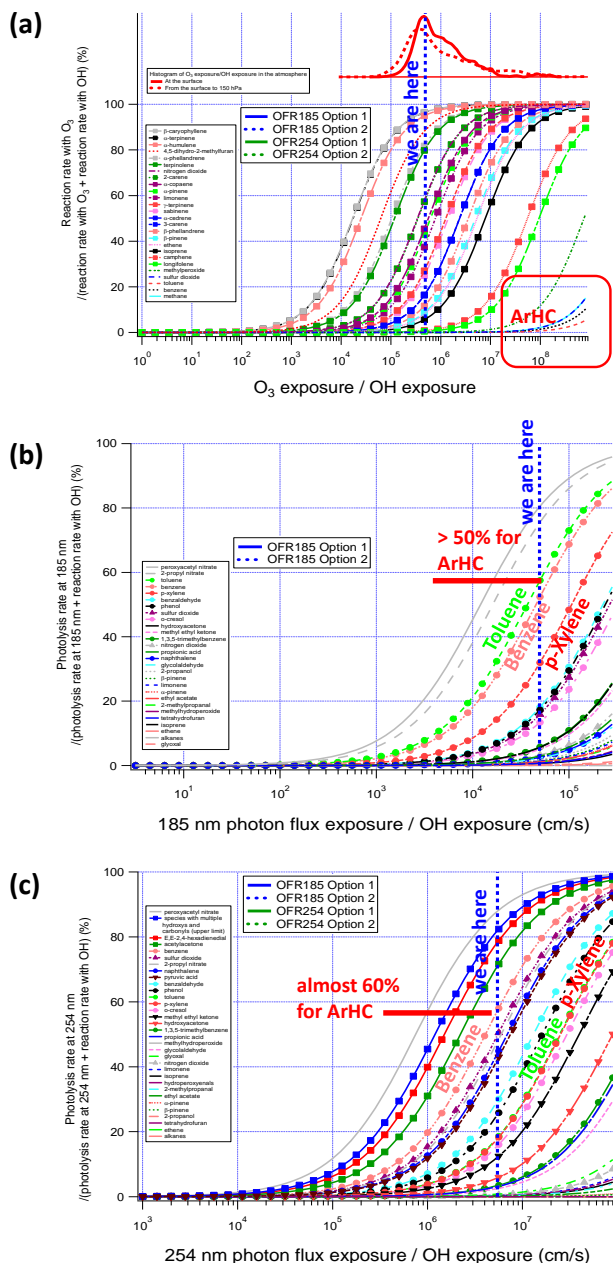


Figure S12. Online OFR: Non-OH loss estimation (Peng et al. OFR model (Peng et al., 2016)). Time-resolved OFR Expts at 100% UV intensity (GDI1, 1 ejector dilution). (a) O₃, (b) 185 nm, (c) 254 nm; please refer to Peng et al. for the legend.(Peng et al., 2016). Input parameters to “2016-10-12_OFR_Exposures_Estimator_v2.3”: OHExt=1000 s⁻¹, [O₃]=1.97x10¹⁴ molec cm⁻³, water mixing ratio=0.005 (0.5% absolute humidity), residence time=100 s; model-predicted OH-exposure=(5.9)x10¹⁰ molec cm⁻³ s.

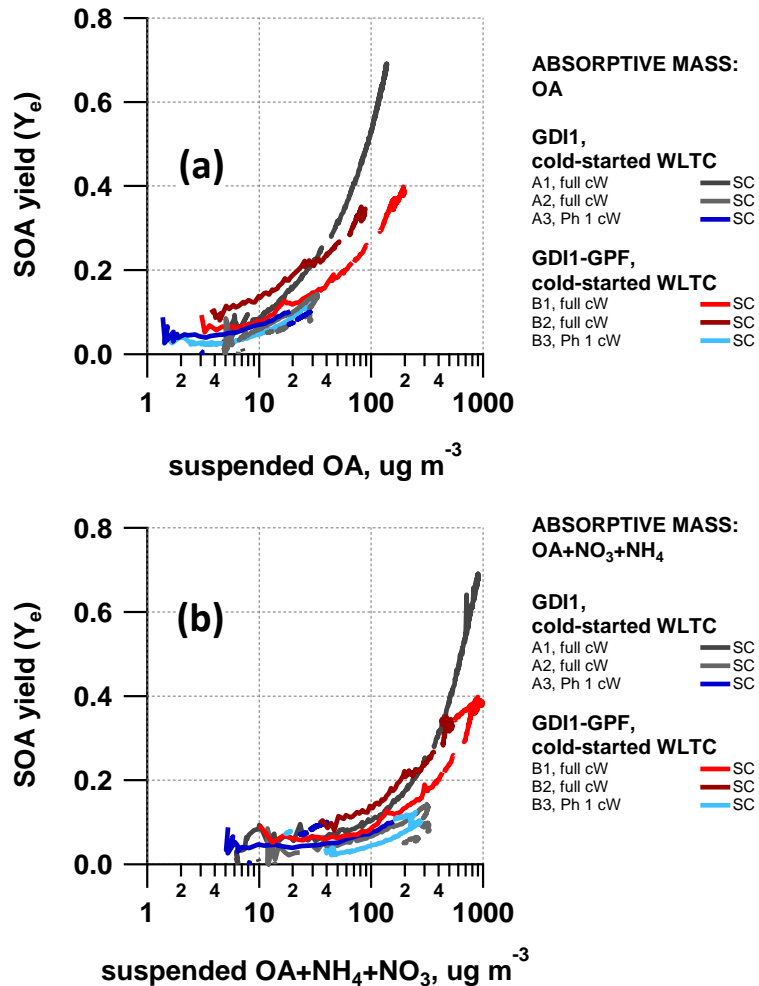


Figure S13. Effective SOA yields from SC experiments with different assumptions of absorptive mass. (a) Yields as a function of suspended OA concentration, and (b) as a function of the sum of OA, HR-ToF-AMS derived ammonia (NH₄) and nitrate (NO₃), assuming that NH₄NO₃ acts as additional absorptive mass. Identifiers (A1-A3, B1-B3) allow retrieving the SC experimental conditions for each experiment from Table S4-S7.

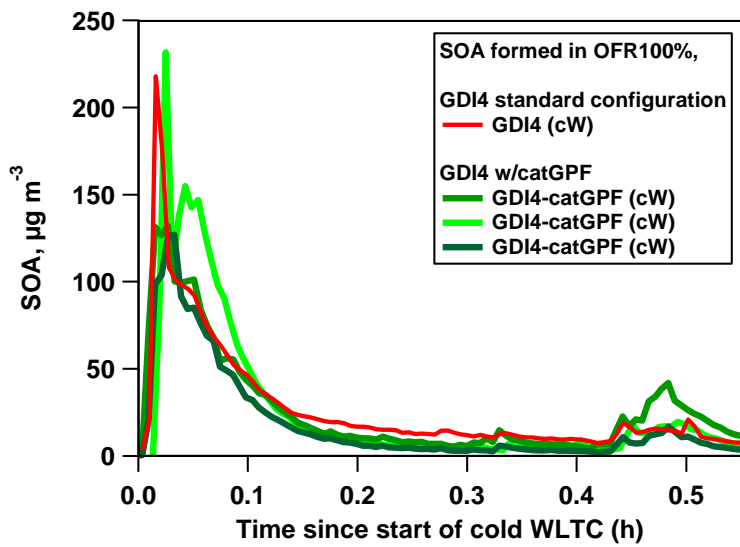


Figure S14. Time-resolved SOA from GDI4 in standard configuration and equipped with a prototype, catalytically active GPF. SOA was generated by exposure of emissions to photochemistry in the OFR during cold-started WLTC test bench experiments.

5

10

18

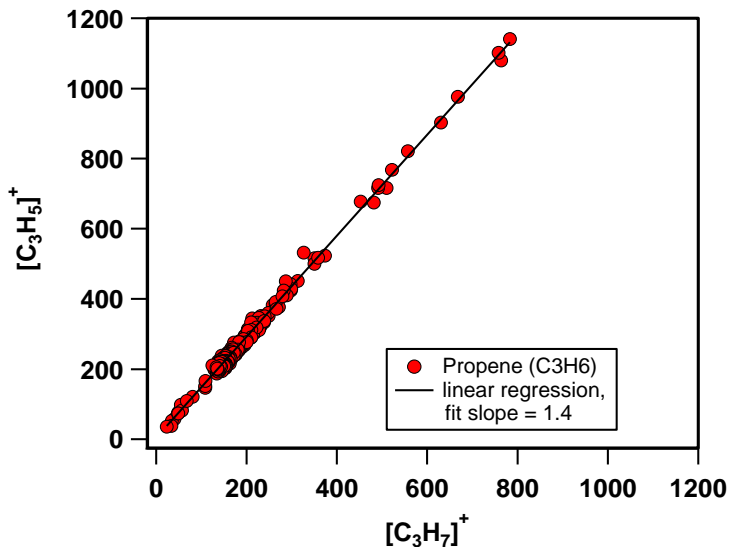


Figure S15. Propene fragmentation ratio in the PTR-ToF-MS. Measurements were conducted at a concentration of around 0-150 ppbv propene (C_3H_6), as measured by the FID instrument.

5

10

19

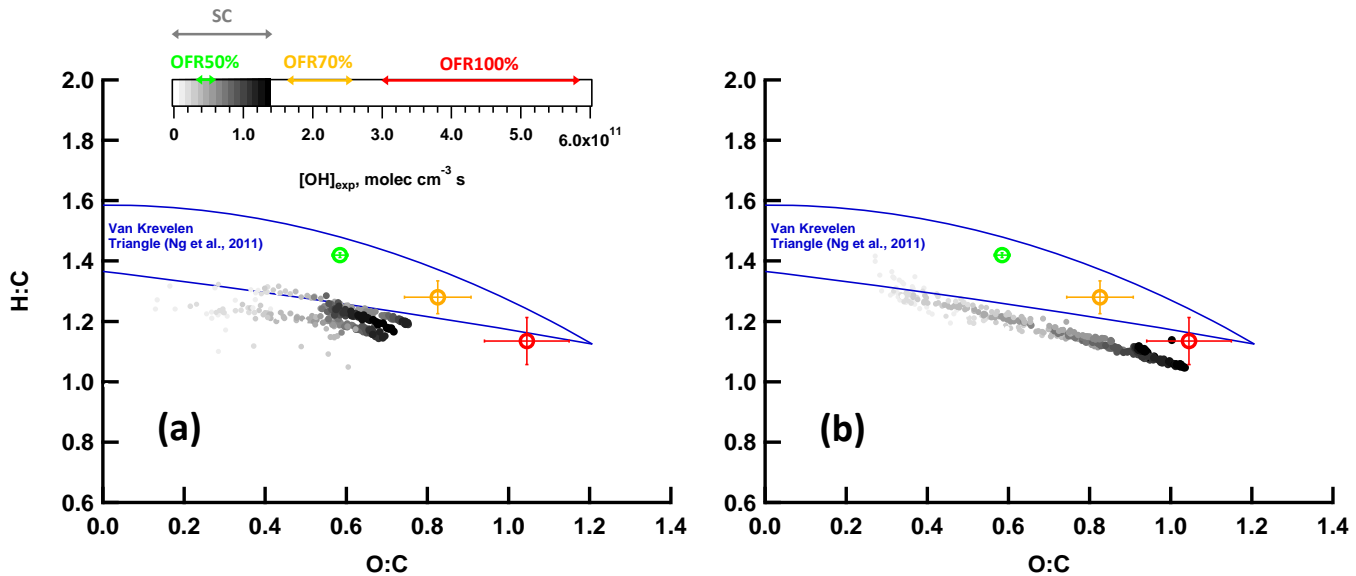


Figure S16. Bulk OA composition of SC and OFR SOA as presented in the main text (Figure 7), here split into (a) SC Expt (2014-05-21, -23, -28, i.e. A2, A3, B3, n=3) and (b) SC Expt (2014-05-20, -26, -27, i.e. A1, B1, B2, n=3). Please refer to the figure legend and the caption in the main text, as well as see also Supporting Information, Table S4-S7, for SC experimental conditions.

5

10

20

3 Tables (Supporting Information)

Table S1. Vehicle specifications.

Parameters	GDI1	GDI2	GDI3	GDI4
Vehicle Type	Opel Insignia 1.6 EcoFlex	Opel Zafira Tourer	VW Golf Plus	Volvo V60 T4F
Engine code	A16XHT	A16XHT	CAV	B4164T2
Cylinder (number/arrangement)	4 / in line	4 / in line	4 / in line	4 / in line
Displacement,cm3	1598	1598	1390	1596
Power, kW	125 @ 6000 rpm	125 @ 6000 rpm	118 @ 5800 rpm	132 @ 5700 rpm
Torque, Nm	260 @ 1650-3200 rpm	260 @ 1650 - 3200 rpm	240 @ 1500 rpm	240 @ 1600 rpm
Injection type	DI	DI	DI	DI
Curb weight, kg	1701	1678	1348 - 1362	1554
Gross vehicle weight, kg	2120	2360	1960 - 1980	2110
Drive wheel	Front-wheel drive	Front-wheel drive	Front-wheel drive	Front-wheel drive
Gearbox	m6	m6	m6	a6
First registration	2014	22.07.2014	01.02.2010	27.01.2012
Exhaust	EURO 5b+	EURO 5b+	EURO 4	EURO 5a
VIN	YV1FW075BC1043598	WOLPD9EZ0E2096446	WVWZZZ1KZ9W844855	YV1FW075BC1043598

Table S2. Gas-phase instrumentation.

Gas phase	Measured	Manu-facturer	Lower limit / Range
Instrument	Parameter		
Picarro Cavity Ring-Down Spectrometer G2401	$\text{CO}_2 + \text{CO} + \text{CH}_4 + \text{H}_2\text{O}$	Picarro	0 - 1000 ppmC (CO_2) 0 - 5 ppmC (CO) 0 - 20 ppmC (CH_4) 0 - 7% (H_2O)
THC Monitor APHA-370	Total Hydrocarbon (THC), Non-methane hydrocarbon (NMHC)	Horiba	0.02 - 100 ppmC
High Resolution-Proton-Transfer-Reaction-Time-of-Flight-Mass Spectrometer (HR-PTR-ToF-MS)	Trace volatile organic compounds (VOCs)	Ionicon Analytik	10ppt -1ppm

5 Table S3. Particle-phase instrumentation.

Particle Phase	Measured	Manu-facturer	Lower limit / Range
Instrument	Parameter		
High Resolution-Aerosol-Time-of-Flight-Mass Spectrometer (HR-ToF-AMS)	Size resolved non-refractory particulate matter (mainly organics)	Aerodyne	$<1\mu\text{g m}^{-3}$ / d_p 0.1-1 μm
Scanning Mobility Particle Sizer (SMPS)	Number-weighted aerosol size distribution	Home built, with TSI DMA, and 3022 CPC	0.01 cm^{-3} , d_p 15-850nm
Aethalometer AE33	Equivalent Black Carbon (eBC)	Aerosol d.o.o	30 ng m^{-3} , $10 \text{ ng m}^{-3} - 100 \text{ ng m}^{-3}$
Condensation particle counter CPC 3776	Particle number	TSI	$4 \text{ nm}, 0.01-10^7 \text{ particles cm}^{-3}$

Table S4. Average concentration after sampling into the SC, formed in the SC or OFR-from-SC (GDI1, cold-started WLTC and EDC).

Expt	Veh.	Test cycle [#]	Ph	NMHC (FID)		CO	CO ₂	NO _x	NMHC/NO _x	NMOC (PTR)	NMOC (PTR)	ArHC (PTR)	eBC	POA	SOA*	Nitrate*
				ppbC	ppbC	ppm	ppm	ppb	ppb ⁻¹	μg m ⁻³	μgC m ⁻³	μg m ⁻³				
A1	GDI1	cW	full	1610	47	1717	72	22	586	462	358	58	6.4	134	606	
			cW												(128'')	(134'')
A2	GDI1	cW	full	1700	36	1909	62	27	575	180	428	53	5.7	32	217	
			cW												(266'')	(185'')
A3	GDI1	cW	Ph 1	2280	17	700	25	91	762	670	669	33	2.8	61	29.9	
			Ph 2-4												(275'')	(99'')
A4	GDI1	cW	Ph 2-4	274	24	1328	33	8	146	93	26	9.7	1.9	2.8	198	
															(5.4'')	(50'')
B1	GDI1- GPF	cW	full	2400	41	2123	58	41	891	776	759	0.05	2.4	195	625	
			cW												(486'')	(185'')
B2	GDI1- GPF	cW	full	1800	29	1766	56	32	558	481	458	0.05	3.3	87	347	
			cW												(305'')	(156'')
B3	GDI1- GPF	cW	Ph 1	1540	15	592	23	66	433	370	361	0.2	1.4	28	189	
			Ph 2-4												(206'')	(99'')
B4	GDI1- GPF	cW	Ph 2-4	182	21	1240	47	4	16	12	4	0.2	1.6	2.5	64	
															(12'')	(144'')
C1	GDI1	cE	full	1870	12	1304	41	46	440	390	391	21	3.7	120 [“]	19 [“]	
			cE													
D1	GDI1- GPF	cE	full	1830	12	1235	32	58	479	413	397	0.05	1.4	239 [“]	43 [“]	
			cE													
D2	GDI1- GPF	cE	full	1770	12	1250	34	52	457	396	388	n.a.	1.5	255 [“]	86 [“]	
			cE													
D3	GDI1- GPF	cE	full	2020	14	1650	38	53	497	439	447	0.05	1.2	255 [“]	57 [“]	
			cE													

⁵ [#]cW refers to cold-started WLTC, cE refers to cold-started EDC cycle; the driving tests were conducted over the full cycle, Ph 1, Ph 2-4 and “full” indications refer to selective sampling of driving cycle phases into the SC and hence presents average exhaust gas concentrations as input to SC (A1-B4) and OFR-from-SC (A1-D3) photochemical experiments. Online time-resolved tests were monitored and emissions were photochemically aged in the OFR over the full driving cycle for each driving test (integrated data are, however, not presented herein except for GDI4 in 2015). *secondary aerosol mass formed upon simulated photochemistry (SC experiments, “OFR-from-SC experiments UV100), not wlc). n.a.=data not available.

Table S5. Average concentration after sampling into the SC, formed in OFR-from-SC (GDI2, cold-started WLTC).

Expt	Veh.	Test cycle [#]	Ph	NMHC (FID) ppbC	CO ppm	CO ₂ ppm	NO _x ppb	NMHC/ NO _x ppbC ppb ⁻¹	NMOC (PTR) μg m ⁻³	NMOC (PTR) μgC m ⁻³	ArHC (PTR) μg m ⁻³	eBC μg m ⁻³	POA μg m ⁻³	SOA* μg m ⁻³	Nitrate* μg m ⁻³
E1	GDI2	cW	full cW	996	8.05	1334	n.a.	n.a.	634	460	315	n.a.	3.5	70 [“]	10 [“]
E2	GDI2	cW	full cW	1430	12.7	1303	n.a.	n.a.	771	575	412	25.1	3.9	129 [“]	24.6 [“]
E3	GDI2	cW	full cW	n.a.	8.4	1003	n.a.	n.a.	504	400	265	9.07	2.1	94 [“]	33.1 [“]
E4	GDI2	cW	Ph 1	n.a.	7.6	398	n.a.	n.a.	378	332	326	7.64	1.1	118 [“]	29.5 [“]

[#]cW refers to cold-started WLTC, cE refers to cold-started EDC cycle; the driving tests were conducted over the full cycle, Ph 1, Ph 2-4 and “full” indications refer to selective sampling of driving cycle phases into the SC and hence presents average exhaust gas concentrations as input to OFR-from-SC photochemical experiments. Online time-resolved tests were monitored and emissions were photochemically aged in the OFR over the full driving cycle for each driving test (integrated data are, however, not presented herein except for GDI4 in 2015). *secondary aerosol mass formed upon simulated photochemistry (“OFR-from-SC experiments UV100). n.a.=data not available.

Table S6. Average concentration after sampling into the SC, formed OFR-from-SC (GDI3, cold-started WLTC).

Expt	Veh.	Test cycle [#]	Ph	NMHC (FID) ppbC	CO ppm	CO ₂ ppm	NO _x ppb	NMHC/ NO _x ppbC ppb ⁻¹	NMOC (PTR) μg m ⁻³	NMOC (PTR) μgC m ⁻³	ArHC (PTR) μg m ⁻³	eBC μg m ⁻³	POA μg m ⁻³	SOA* μg m ⁻³	Nitrate* μg m ⁻³
F1	GDI3	cW	full cW	1198	10.0	525	n.a.	n.a.	447	380	264	13.9	0.48	123 [“]	267 [“]
F2	GDI3	cW	full cW	n.a.	2.07	485	n.a.	n.a.	229	147	137	8.03	0.96	31.2 [“]	42.4 [“]
F3	GDI3	cW	Ph 1	n.a.	1.47	158	n.a.	n.a.	202	154	121	5.45	1.06	26.4 [“]	52.2 [“]
F4	GDI3	cW	Ph 2-4	n.a.	0.49	339	n.a.	n.a.	191	101	33	2.16	0.05	2.3 [“]	65.1 [“]

[#]cW refers to cold-started WLTC, cE refers to cold-started EDC cycle; the driving tests were conducted over the full cycle, Ph 1, Ph 2-4 and “full” indications refer to selective sampling of driving cycle phases into the SC and hence presents average exhaust gas concentrations as input to OFR-from-SC photochemical experiments. Online time-resolved tests were monitored and emissions were photochemically aged in the OFR over the full driving cycle for each driving test (integrated data are, however, not presented herein except for GDI4 in 2015). *secondary aerosol mass formed upon simulated photochemistry (“OFR-from-SC experiments UV100).

n.a.=data not available.

Table S7. Average concentration after sampling into the SC, formed in SC (GDI4, cold-started WLTC).

Expt	Veh.	Test cycle [#]	Ph	NMHC (FID) ppbC	CO ppm	CO ₂ ppm	NO _x ppb	NMHC/ NO _x ppbC ppb ⁻¹	NMOC (PTR) μg m ⁻³	NMOC (PTR) μgC m ⁻³	ArHC (PTR) μg m ⁻³	eBC μg m ⁻³	POA μg m ⁻³	SOA* μg m ⁻³	Nitrate* μg m ⁻³
G1	GDI4	cW	full cW	438	6.01	1218	n.a.	n.a.	429	180	169	9.99	n.a.	10.1	9.1
G2	GDI4	cW	full cW	486	7.03	1555	57	8.5	415	136	177	10.1	2.11	5.1	8.8
G3	GDI4	cW	full cW	750	10.1	1830	112	6.7	508	288	251	14.9	3.05	4.5	27.5
G4	GDI4	cW	full cW	688	n.a.	n.a.	118	5.8	356	215	185	20.1	n.a.	n.a.	n.a.

[#]cW refers to cold-started WLTC, cE refers to cold-started EDC cycle; the driving tests were conducted over the full cycle. Online time-resolved tests were monitored and emissions were photochemically aged in the OFR over the full driving cycle for each driving test (integrated data are, however, not presented herein except for GDI4 in 2015, which are labelled “online OFR” in the corresponding figures in the main text). *secondary aerosol mass formed upon simulated photochemistry (SC experiments, not wlc). n.a.=data not available.

References (Supporting Information)

Barmet, P., Dommen, J., DeCarlo, P. F., Tritscher, T., Praplan, A. P., Platt, S. M., Prévôt, A. S. H., Donahue, N. M., and Baltensperger, U.: OH clock determination by proton transfer reaction mass spectrometry at an environmental chamber, *Atmos. Meas. Tech.*, 5, 647-656, 10.5194/amt-5-647-2012, 2012.

5

Bruns, E. A., El Haddad, I., Keller, A., Klein, F., Kumar, N. K., Pieber, S. M., Corbin, J. C., Slowik, J. G., Brune, W. H., Baltensperger, U., and Prévôt, A. S. H.: Inter-comparison of laboratory smog chamber and flow reactor systems on organic aerosol yield and composition, *Atmos. Meas. Tech.*, 8, 2315-2332, 10.5194/amt-8-2315-2015, 2015.

10 IUPAC: Task Group on Atmospheric Chemical Kinetic Data Evaluation, online at: <http://iupac.pole-ether.fr/>. IUPAC Task Group on Atmospheric Chemical Kinetic Data Evaluation – Data Sheet HOx_VOC10 (data sheet last updated 12th January 2005).

15 Li, R., Palm, B. B., Ortega, A. M., Hlywiak, J., Hu, W., Peng, Z., Day, D. A., Knot, C., Brune, W. H., de Gouw, J. A., and Jimenez, J. L.: Modeling the radical chemistry in an oxidation flow reactor: radical formation and recycling, sensitivities, and the OH exposure estimation equation, *J Phys Chem A*, 119, 4418-4432, 10.1021/jp509534k, 2015.

20 Peng, Z., Day, D. A., Stark, H., Li, R., Lee-Taylor, J., Palm, B. B., Brune, W. H., and Jimenez, J. L.: HOx radical chemistry in oxidation flow reactors with low-pressure mercury lamps systematically examined by modeling, *Atmos. Meas. Tech.*, 8, 4863-4890, 10.5194/amt-8-4863-2015, 2015.

25 Peng, Z., Day, D. A., Ortega, A. M., Palm, B. B., Hu, W., Stark, H., Li, R., Tsigaridis, K., Brune, W. H., and Jimenez, J. L.: Non-OH chemistry in oxidation flow reactors for the study of atmospheric chemistry systematically examined by modeling, *Atmos. Chem. Phys.*, 16, 4283-4305, 10.5194/acp-16-4283-2016, 2016.

Peng, Z., and Jimenez, J. L.: Modeling of the chemistry in oxidation flow reactors with high initial NO, *Atmospheric Chemistry and Physics Discussions*, 1-37, 10.5194/acp-2017-266, 2017.

30 Pieber, S. M., El Haddad, I., Slowik, J. G., Canagaratna, M. R., Jayne, J. T., Platt, S. M., Bozzetti, C., Daellenbach, K. R., Frohlich, R., Vlachou, A., Klein, F., Dommen, J., Miljevic, B., Jimenez, J. L., Worsnop, D. R., Baltensperger, U., and Prévôt, A. S. H.: Inorganic Salt Interference on CO_2^+ in Aerodyne AMS and ACSM Organic Aerosol Composition Studies, *Environ Sci Technol*, 50, 10494-10503, 10.1021/acs.est.6b01035, 2016.

35 Platt, S. M., El Haddad, I., Zardini, A. A., Clairotte, M., Astorga, C., Wolf, R., Slowik, J. G., Temime-Roussel, B., Marchand, N., Ježek, I., Drinovec, L., Močnik, G., Möhler, O., Richter, R., Barmet, P., Bianchi, F., Baltensperger, U., and Prévôt, A. S. H.: Secondary organic aerosol formation from gasoline vehicle emissions in a new mobile environmental reaction chamber, *Atmos. Chem. Phys.*, 13, 9141-9158, 10.5194/acp-13-9141-2013, 2013.

40 Platt, S. M., El Haddad, I., Pieber, S. M., Zardini, A. A., Suarez-Bertoa, R., Clairotte, M., Daellenbach, K. R., Huang, R. J., Slowik, J. G., Hellebust, S., Temime-Roussel, B., Marchand, N., de Gouw, J., Jimenez, J. L., Hayes, P. L., Robinson, A. L., Baltensperger, U., Astorga, C., and Prévôt, A. S. H.: Gasoline cars produce more carbonaceous particulate matter than modern filter-equipped diesel cars, *Sci Rep*, 7, 4926, 10.1038/s41598-017-03714-9, 2017.

45